INDC International Nuclear Data Committee

Articles Translated from Journal Yadernye Konstanty (Nuclear Constants)

(Series: Nuclear Constants, Issue No. 1–2, 2005)

Translated by the IAEA

April 2007

Articles Translated from Journal Yadernye Konstanty (Nuclear Constants)

(Series: Nuclear Constants, Issue No. 1–2, 2005)

Translated by the IAEA

Abstract

This report contains the translation of three papers published in the Nuclear Constants journal (Voprosy Atomnoj Nauki I Teknniki, seriya: Yadernye Konstanty (YK), vypusk 1–2, 2005).

April 2007

TABLE OF CONTENTS

EVALUATION OF THE [248]Cm RESOLVED RESONANCE REGION

G.B. Morogovskij, L.A. Bakhanovich
Sosny Joint Institute for Energy and Nuclear Research, Belarus National Academy of Sciences

EVALUATION OF THE [248]Cm RESOLVED RESONANCE REGION. Thermal cross-sections, a set of Breit-Wigner parameters and background cross-sections for the representation of $\sigma_t(E)$, $\sigma_\gamma(E)$ and $\sigma_f(E)$ energy dependence in the 10^{-5}–2150 eV region have been obtained as a result of the evaluation of measured resonance integrals and experimental cross-sections at 0.0253 eV and fission cross-sections in the 0.1–2640 eV energy region.

Analysis of the existing ENDF/B-VI and JENDL-3.3 evaluated nuclear data files in the [248]Cm resolved resonance region of interest to us shows that these evaluations are essentially based on the same resonance parameters [1,2] except that, in the JENDL-3.3 evaluation, the parameters of a number of low-lying resonances were changed somewhat to take into account the measurements in [3]. The upper boundary of the resolved resonance region was taken to be 2400 eV in the ENDF/B-VI file and 1500 eV in the JENDL-3.3 file. We did not examine the JEF-2 file because, in the resolved resonance region, it coincides with the ENDF/B-VI file. Comparison of the experimental fission cross-sections [2,3] and those calculated according to the files with account taken of the experimental conditions shows that there are marked discrepancies, not only between the measured and the calculated cross-sections, but also between the sets of experimental data themselves. The aim of this paper is to obtain a set of Breit-Wigner resonance parameters that, as far as possible, adequately reproduce all the existing experimental cross-sections in the resolved resonance region.

Initially, we took the upper boundary of the resolved resonance region to be 2640 eV because the available experimental data [2] do not allow reliable identification of resonances above this energy. It should be noted that, when performing the parametrization, we used only the authors' values for the cross-sections and no evaluation was carried out at the parameter level. The calculations were based on the evaluated values given in Table 1 for the thermal cross-sections and resonance integrals, obtained on the basis of the corresponding measurements, and also experimental data for $\sigma_f(E)$ and $\sigma_\gamma(E)$ [2,3] taken from EXFOR.

For the region under investigation we used the available experimental data from the EXFOR library. These data are from publications [2,3]. It should be noted that these papers cover the entire resolved resonance region, but the quality of the cross-section measurements is very variable. The summarized results of analysis of these experimental data are given below:

1. $\sigma_f(E)$ — paper by Moore and Keyworth [2], in which the cross-section is measured in a nuclear explosion experiment starting at 20 eV; the good energy resolution of the experiment allows these data to be used for parametrization up to 2640 eV, but the large number of energy points where the cross-sections are negative (more than 30%) arouse suspicion;

2. $\sigma_\gamma(E)$ — paper by Moore and Keyworth [2], the radiative capture cross-sections are given only for three strong resonances (26.9, 76.1 and 98.95 eV);

3. $\sigma_f(E)$ — paper by Maguire et al. [3], in which the cross-section is measured starting at 0.13 eV, but the energy resolution is such that only data up to 100 eV can be used directly to calculate the parameters.

As the starting set of parameters we took the scattering radius and the parameters of the most recent and most complete evaluation — JENDL-3.3, containing 47 resonances in the 10^{-5} – 3000 eV range, which are a combination of papers [1-3], without using the smooth background cross-section given in the evaluation.

Evaluation of missing resonances for the starting set of parameters leads to the conclusion that there must be quite a number of missing resonances, both because of the smallness of the neutron widths and the energy resolution, particularly above 700 eV, fairly strong resonances may be omitted. Comparison of the experimental cross-sections in [2,3] with the cross-sections calculated using the starting set parameters, taking into account the actual energy resolution in the 1–2400 eV region, showed that:

1. To obtain the resonance parameters in the 0.1–20 eV range the $\sigma_f(E)$ data [3] can be used, in the 20–100 eV range the $\sigma_f(E)$ data in both [2 and 3] can be used, and above 100 eV only the data in [2] are suitable to calculate the parameters;

2. The resonance energies of part of the resonances need to be improved, and a number of resonance energies do not correspond at all to the energy dependence of the fission cross-section [2];

3. The neutron widths of most of the resonances are clearly too high, and the fission widths of resonances above 259 eV are taken to be 1.3 MeV (except for the five resonances in the 457–650 eV region, to which a width of 1 MeV is assigned), as a result of which almost all the resonances above 235 eV have values of $\sigma^0_f(E_r)$ that are unreasonably high;

4. A fairly large number of previously unidentified weak resonances can be identified and their parameters calculated, thereby allowing the description of all the experimental data to be improved.

Figs. 1–5 give the experimental and calculated cross-section values, illustrating the conclusions that can be drawn.

In this paper the resonance parameters were calculated in several stages, using the shape method. First of all, using the available experimental data in the aforementioned energy ranges, new values were calculated for the neutron, fission and capture widths of the resonances included in the starting set and, at the same time, their resonance energies were corrected. In this case, the Γ_γ magnitudes could be determined only for a number of low-lying resonances while all the rest were given the average value $\Gamma_\gamma=20.4$ MeV, obtained through calculation. Then, a comparative analysis was carried out of the energy dependence of the experimental and calculated cross-sections $\sigma_f(E)$, enabling a fairly large number of previously unidentified resonances to be detected and their resonance energies determined. After this, the neutron and fission widths of these resonances were calculated and, at the same time, their resonance energies corrected. Lastly, a final corrective calculation of the parameters of all the resonances in the 0.1–2640 eV range was performed. In the final stage, using the evaluated values given in Table 1, the parameters of the negative resonance, which basically determines the cross-section values at the thermal point, were calculated.

Table 1. Thermal cross-sections and resonance integrals for ^{248}Cm (barns)

Ref.	σ_γ	σ_f	I_γ	I_f
[4]	7.2±2.0 (SPA)		350±40	
[5]	2.63 (MXW)		267	
[6]	6.0 (SPA)			
[7]	10.7±1,5		250±24	
[8]	4.0 (SPA)			
[9]		0.34±0.07		13.2±0.8
[10]		0.39±0.07		13.1±1.5
Evaluated value	10.7±1.5	0.365±0.049	276.5±20.6	13.178±0.706

When determining the position of and calculating the resonance parameters of previously unidentified resonances, there is always a danger of taking a distortion in the experimental data to be a resonance, especially if the calculation is performed on the basis of one type of cross-section, and all the more so if it is based on one measurement. Since, in this paper, the position and parameters of previously unidentified resonances above 100 eV were determined only on the basis of a fission cross-section [2], by way of control we used a comparison of the fission cross-section calculated using our parameters with the data in [3]. This approach significantly reduced the inclusion of "superfluous" resonances in the set.

Comparison of Figures 1 and 5 shows that the calculation using our parameters satisfactorily reproduces the measurements in [2] up to 2640 eV, whereas agreement with experiment [3] above 2150 eV starts to deteriorate because of the increasing number of missing, fairly strong, resonances. Thus, we recommend that the results of the present paper be used up to 2150 eV.

Table 2 gives the parameters of 193 resonances obtained by us, and Table 3 the average resonance parameters and thermal cross-sections calculated using them. For comparison, this Table gives the corresponding magnitudes calculated using the ENDF/B-VI and JENDL-3.3 files. It can be seen that the thermal cross-sections in our paper accurately reproduce the evaluated values from Table 1 with the exception of I_f.

9

Table 2. Resonance parameters for ^{248}Cm

E_r, eV	Γ_n, meV	Γ_γ, meV	Γ_f, meV	E_r, eV	Γ_n, meV	Γ_γ, meV	Γ_f, meV
-0.50	0.013392	20.40	1.11290	236.30	92.2620	20.40	0.18720
0.60	0.0064392	21.40	0.07509	237.640	12.3170	20.40	0.38094
1.430	0.00062733	20.40	2.66940	245.50	8.02350	20.40	0.04140
4.50	0.028084	28.40	0.64262	253.150	47.7550	20.40	0.02763
7.264	0.29354	23.30	0.32579	257.750	96.3810	20.40	0.04941
11.30	0.57645	20.40	0.02355	268.850	8.0230	20.40	0.05664
16.80	0.47366	20.40	0.12634	273.520	99.2770	20.40	0.00853
26.850	90.0190	14.40	0.05183	277.260	0.32333	20.40	1.12160
35.010	0.40991	19.20	0.31215	289.10	23.3180	20.40	0.04166
36.620	0.10734	18.50	0.37016	291.050	51.1970	20.40	0.03125
43.150	0.41397	20.40	0.07680	295.20	0.84213	20.40	0.70114
45.40	0.08033	20.40	0.23913	299.10	0.34287	20.40	0.48131
47.40	0.52602	20.40	0.11871	308.50	0.74739	20.40	0.83462
49.650	0.49194	20.40	0.14983	316.770	26.6980	20.40	0.03822
53.650	0.45985	14.50	0.15439	321.430	33.9960	20.40	0.09807
58.630	0.5390	19.40	0.43480	334.0	45.6610	20.40	0.05192
63.430	0.49798	18.50	0.16317	337.90	23.8870	20.40	0.07814
76.10	60.4380	19.00	4.31790	347.60	0.91842	20.40	1.27020
84.440	6.47210	18.50	0.01793	351.90	75.0810	20.40	0.03795
92.420	6.47130	18.50	0.01876	362.40	12.4650	20.40	0.07301
98.850	366.660	32.50	0.43229	370.250	1.1310	20.40	1.50880
108.680	4.16510	20.40	0.01549	374.650	38.7230	20.40	0.13586
114.510	11.1820	20.40	0.02157	380.30	7.98850	20.40	0.32161
115.40	47.9960	22.70	0.02938	386.90	1.16330	20.40	1.71890
116.850	0.55510	20.40	0.16747	390.30	3.14160	20.40	0.13353
121.080	4.07770	20.40	0.01073	394.0	19.5730	20.40	0.18332
125.80	0.56068	20.40	0.16944	398.50	19.6050	20.40	0.03712
130.180	0.5710	20.40	0.14559	402.0	30.0440	20.40	0.07623
135.250	0.58072	20.40	0.24751	406.0	3.52450	20.40	0.41172
138.310	0.89545	20.40	0.29279	410.70	41.7290	20.40	0.07047
140.050	33.4780	22.70	0.20385	415.20	31.1410	20.40	0.27359
149.410	3.73550	20.40	0.06184	419.250	31.7090	20.40	0.05890
150.370	7.10390	20.40	0.02927	426.0	82.5780	20.40	0.04884
158.450	1.1040	20.40	0.20082	443.070	35.5750	20.40	0.13568
164.90	0.28835	20.40	0.80867	456.870	25.3370	20.40	0.16045
181.40	33.6850	20.40	0.03569	460.720	11.9420	20.40	0.60918
183.0	0.38306	20.40	2.63720	465.410	64.6940	20.40	0.11783
184.60	81.4890	20.40	0.05249	471.10	30.2540	20.40	0.33622
186.0	38.1780	20.40	0.21163	490.150	20.5990	20.40	0.19314
188.30	6.85880	20.40	0.02965	494.350	20.430	20.40	0.08786
192.20	0.69234	20.40	0.23308	503.30	10.9370	20.40	0.68912
196.20	0.41138	20.40	0.98941	509.0	3.91690	20.40	0.62503
209.780	27.9710	20.40	0.00871	512.750	3.94820	20.40	0.60992
212.750	0.43384	20.40	0.51059	516.550	6.59720	20.40	0.23082
214.20	2.77340	18.75	0.07318	521.050	1.00990	20.40	1.26140
218.020	59.020	20.40	0.00276	524.350	1.1940	20.40	1.37780
221.950	29.7830	20.40	0.01425	531.050	1.00560	20.40	2.48530
224.80	75.0	20.40	0.01345	536.20	1.19540	20.40	2.6840
227.70	30.1660	20.40	0.02276	545.60	24.5590	20.40	0.23808
230.10	68.2770	20.40	0.04204	550.50	55.2590	20.40	0.02682
232.60	22.9470	20.40	0.19005	555.70	17.9070	20.40	0.19447

E_r, eV	Γ_n, meV	Γ_γ, meV	Γ_f, meV	E_r, eV	Γ_n, meV	Γ_γ, meV	Γ_f, meV
558.60	11.7970	20.40	0.18020	1160.0	8.47080	20.40	2.21270
564.20	1.23840	20.40	2.78030	1176.60	49.9880	20.40	0.77123
568.750	11.9030	20.40	0.19663	1193.40	84.0150	20.40	1.49020
572.50	12.4360	20.40	0.28295	1229.90	13.8020	20.40	1.01150
582.70	1.64540	20.40	7.71620	1248.30	31.1250	20.40	1.39720
594.50	16.3220	20.40	0.04283	1282.40	9.24880	20.40	2.06770
601.0	49.0270	20.40	0.12401	1293.10	95.6820	20.40	0.04312
609.050	1.59480	20.40	7.84670	1339.20	18.6470	20.40	0.65664
624.0	12.3940	20.40	0.30932	1348.0	12.7050	20.40	1.40470
627.60	15.8030	20.40	0.50582	1416.50	30.0340	20.40	0.30839
634.770	10.0690	20.40	0.15423	1428.70	40.0470	20.40	0.43782
642.850	3.19110	20.40	0.80775	1451.0	39.8560	20.40	1.78140
649.50	17.8260	20.40	0.18709	1481.80	47.0270	20.40	1.00750
653.50	2.08570	20.40	4.20530	1502.50	10.5690	20.40	1.54840
661.250	77.120	20.40	0.39654	1524.0	17.2680	20.40	1.24850
670.50	6.88550	20.40	1.20720	1534.0	37.5180	20.40	0.22164
686.0	73.2470	20.40	0.29289	1595.50	22.1050	20.40	1.69740
693.70	7.65520	20.40	0.72489	1612.70	5.81740	20.40	3.86490
720.80	22.2230	20.40	0.38020	1645.0	32.640	20.40	2.33180
729.90	2.0070	20.40	2.13970	1660.0	29.890	20.40	1.17860
738.920	27.6060	20.40	0.63888	1677.50	68.7750	20.40	1.82160
782.50	13.7950	20.40	0.47675	1710.50	39.8360	20.40	0.49481
789.80	12.070	20.40	0.64759	1739.50	32.1770	20.40	1.70820
800.20	14.1160	20.40	0.43281	1767.0	4.44280	20.40	4.35880
811.80	9.65380	20.40	1.25540	1833.0	68.4030	20.40	2.24280
822.10	46.0880	20.40	0.56381	1971.50	6.21310	20.40	3.75230
833.90	23.090	20.40	0.17943	2002.0	20.6470	20.40	1.76570
841.950	26.0810	20.40	0.12777	2058.50	38.430	20.40	2.7440
851.750	43.7490	20.40	0.34513	2080.0	35.4040	20.40	1.18650
876.60	46.3030	20.40	0.36897	2117.50	46.2920	20.40	2.37850
891.0	104.360	20.40	1.4830	2145.80	6.96560	20.40	6.3180
903.0	27.9860	20.40	0.16346	2180.50	32.0960	20.40	2.84430
933.0	76.2770	20.40	0.20677	2213.50	20.2540	20.40	2.15870
948.10	33.8280	20.40	0.59590	2243.0	35.6650	20.40	3.23070
961.0	27.8460	20.40	0.71548	2258.0	34.7450	20.40	2.8820
973.50	37.40	20.40	0.58663	2298.0	24.1620	20.40	4.58930
995.40	91.3980	20.40	0.69809	2324.0	42.040	20.40	3.45150
1015.20	29.5590	20.40	0.33773	2347.50	31.1460	20.40	1.25610
1029.80	25.8110	20.40	0.55058	2372.0	13.8960	20.40	0.88291
1041.50	10.8340	20.40	0.20813	2403.0	23.3230	20.40	7.33570
1052.0	6.15410	20.40	0.39180	2439.0	4.82750	20.40	2.14960
1103.0	53.2810	20.40	1.57630	2473.0	52.5990	20.40	2.65680
1115.50	6.47740	20.40	0.92980	2508.50	40.8980	20.40	5.33180
1126.50	5.22350	20.40	2.93550	2552.0	37.2960	20.40	4.21580
1139.0	8.3350	20.40	0.71845	2604.0	26.6330	20.40	7.31130
1149.0	73.70901	20.40	0.28304				

The main differences between the average resonance parameters in our paper and those obtained in previous evaluations are the considerably lower values of $<\Gamma_n^0>$ and $<D>$. However, this result did not lead to a noticeable change in S^0 because the omission of the additional resonances discovered by us was due not only to the smallness of the neutron widths of part of them, but also to the energy resolution of the experimental data, referred to above.

The anomalously small calculated value $\sigma_n^{2200} \approx 3.47$ b obtained using our parameters is due to potential scattering and the contribution of all the resonances, set down in Table 2 as follows:

- potential scattering: 10.41 b,

- resonance scattering: 0.38 b,

- interference between potential and resonance scattering: -8.80 b,

- inter-resonance interference: 1.48 b.

The contribution to interference between potential and resonance scattering from the 26.86 eV resonance is -3.39 b, and the contribution from the 98.85 resonance is -1.95 b. Thus, the negative contribution from both of these resonances to the cross-section σ_n^{2200} is -5.34 b, i.e. 60.5% of the total interference between potential and resonance scattering. This contribution is determined by the anomalously large magnitudes of Γ_n^0 for these resonances (17.37 and 36.88 MeV), whereas the magnitude of $<\Gamma_n^0>$ calculated using all the resonances in Table 2 is 1.316 MeV. However, such values of the neutron widths of these resonances are obtained as a result of calculations of the parameters, based on the requirement for a consistent description of all three available series of experimentally measured cross-sections (σ_f (E) and σ_γ (E) [2], and also σ_f (E) [3]) in the energy regions of the given resonances.

As is known in the absence of systematic errors in the experimental data, the cross-sections calculated using the evaluated parameters with account taken of the measurement conditions (assembly energy resolution function, effective temperature, isotopic composition of the sample, etc.), must satisfactorily reproduce the corresponding experimental data used in obtaining the parameters. The calculation, shown in Figs 1–5, of fission cross-sections using the Table 2 parameters for the experiments in [2,3] clearly indicates the presence of a systematic deviation of the calculated values of σ_f (E) from the experimental data in [3], at least in the energy ranges 30–57 eV and 100–550 eV (whereby in the latter case this deviation has a clearly expressed energy dependence), whereas the measurements of σ_f (E) in [2], used to calculate the parameters in the given regions, are reproduced fairly reliably. The calculations of the average cross-sections and fission resonance integrals in the energy ranges for the experimental measurements in [2,3] in the entire resolved resonance region investigated by us indicate that the measurements in [2] lie systematically lower than the measurements in [3].
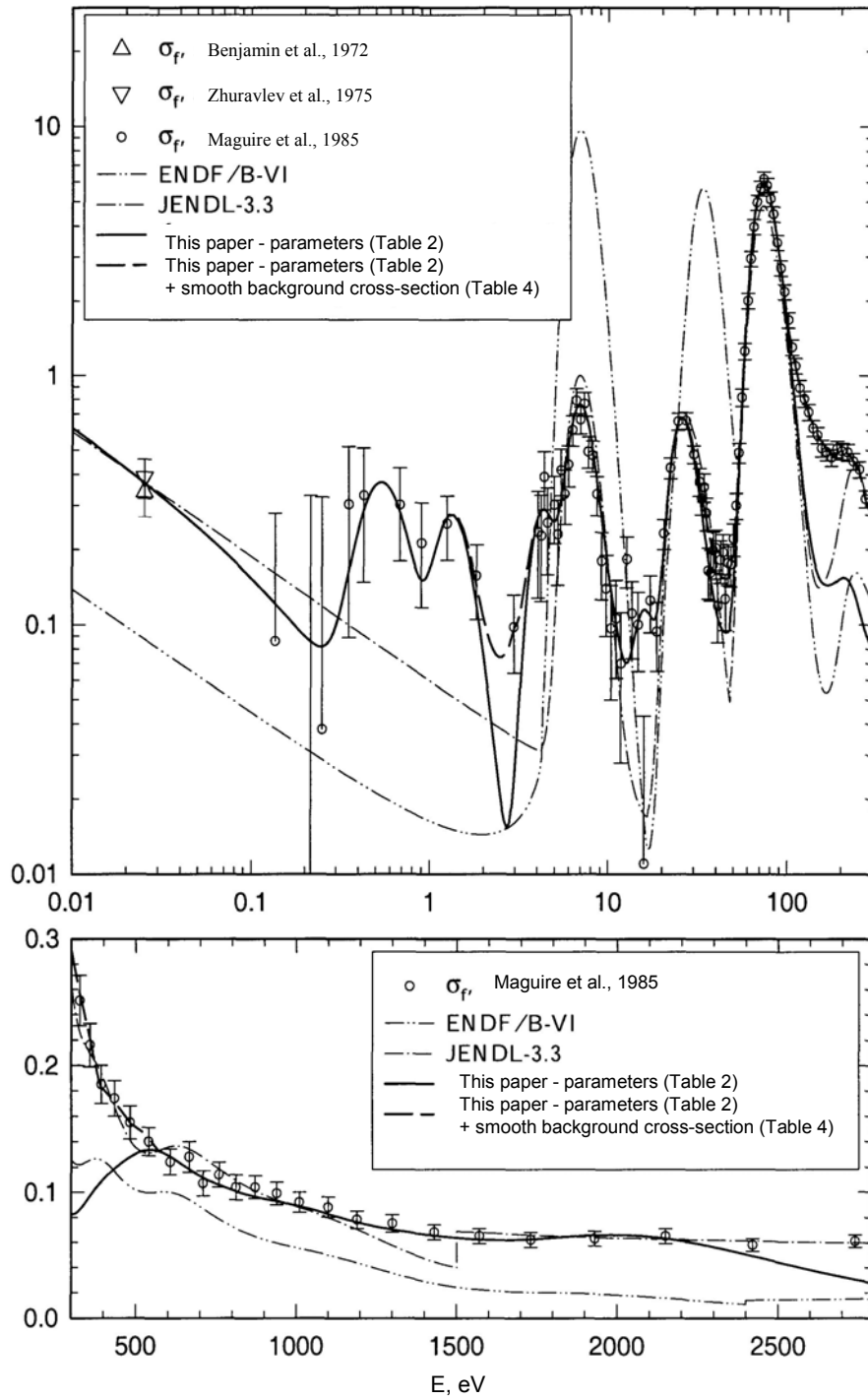
Fig. 1. Comparison of the experimentally measured [3] fission cross-section and the fission cross-sections calculated using the ENDF/B-VI and JENDL-3.3 files and the results of this paper in the 0.01–2800 eV energy range.

13
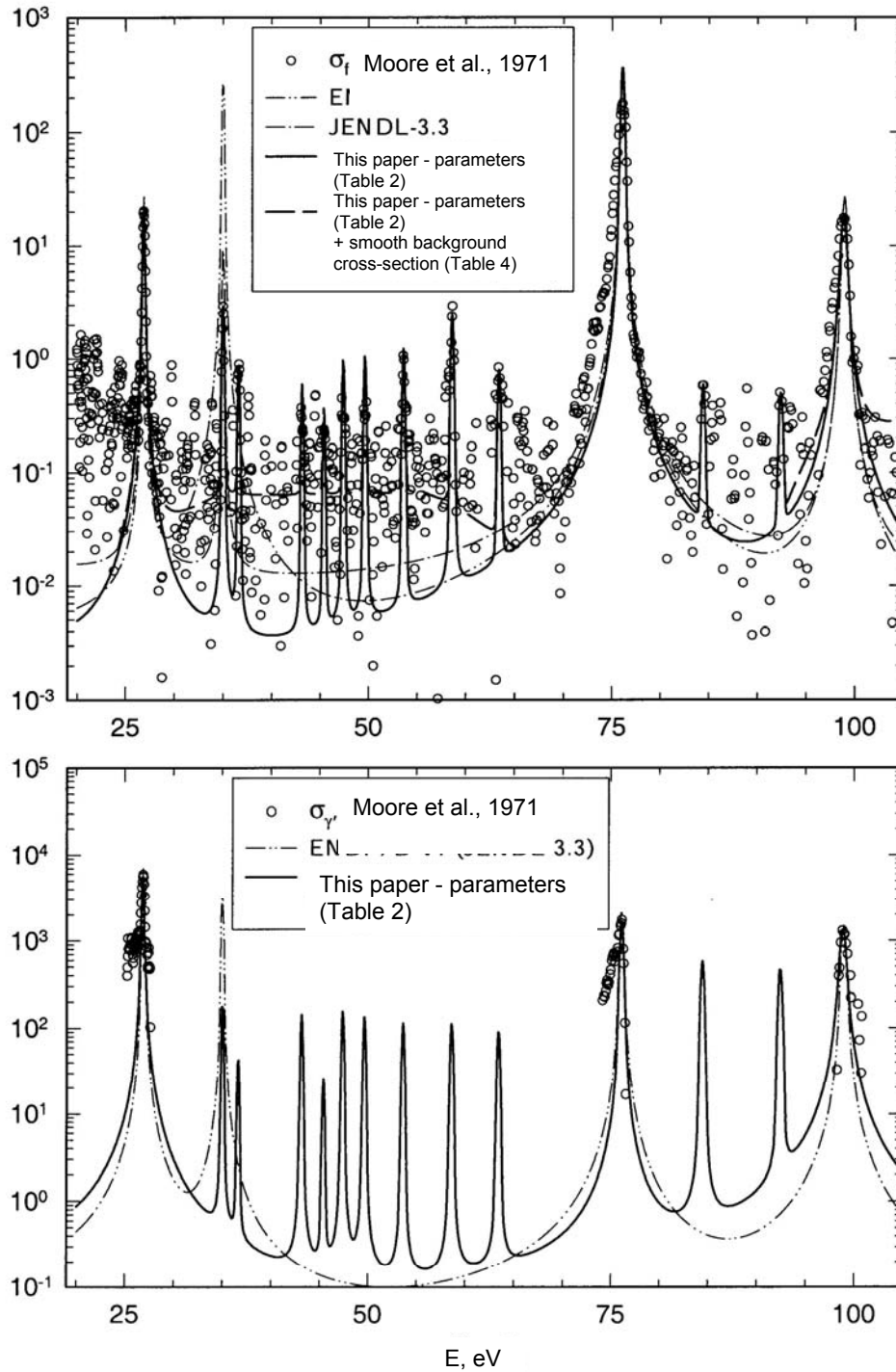
Fig. 2. Comparison of the experimentally measured [2] fission cross-section and the fission cross-sections calculated using the ENDF/B-VI and JENDL-3.3 files and the results of this paper in the 20–105 eV energy range.

14
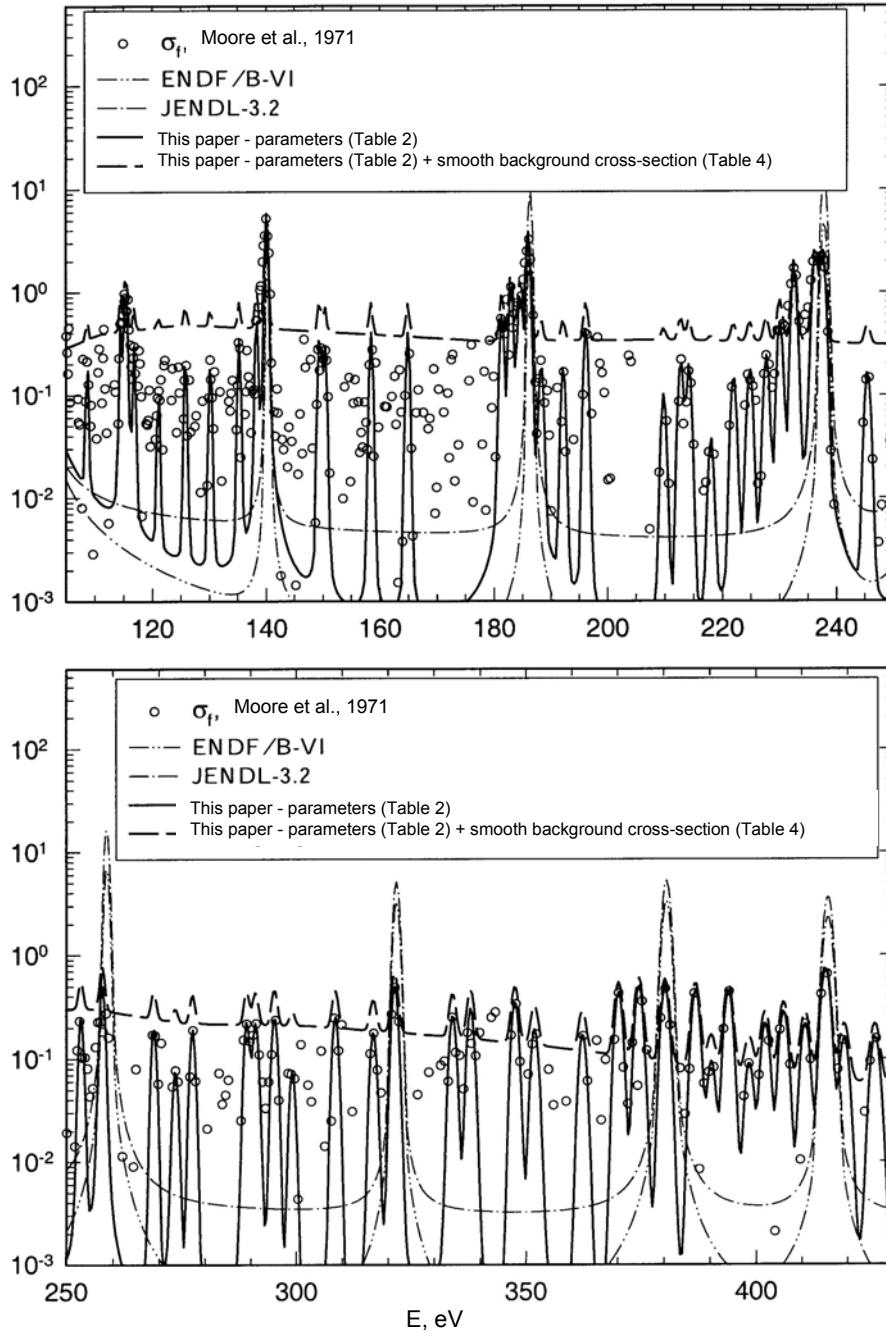
Fig. 3. Comparison of the experimentally measured [2] fission cross-section and the fission cross-sections calculated using the ENDF/B-VI ad JENDL-3.3 files and the results of this paper in the 105–430 eV energy range.
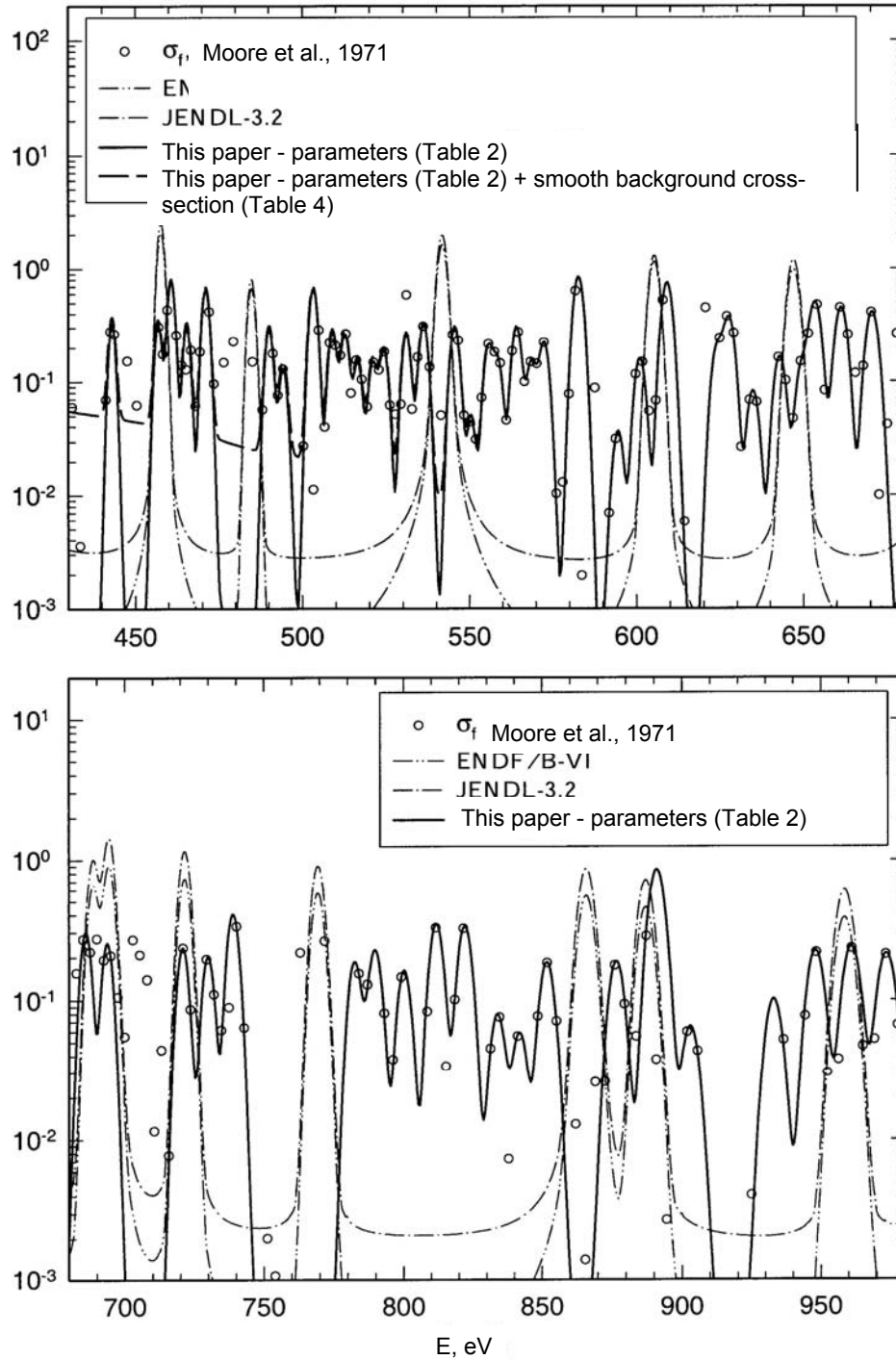
Fig. 4. Comparison of the experimentally measured [2] fission cross-section and the fission cross-sections calculated using the ENDF/B-VI ad JENDL-3.3 files and the results of this paper in the 430–980 eV energy range.
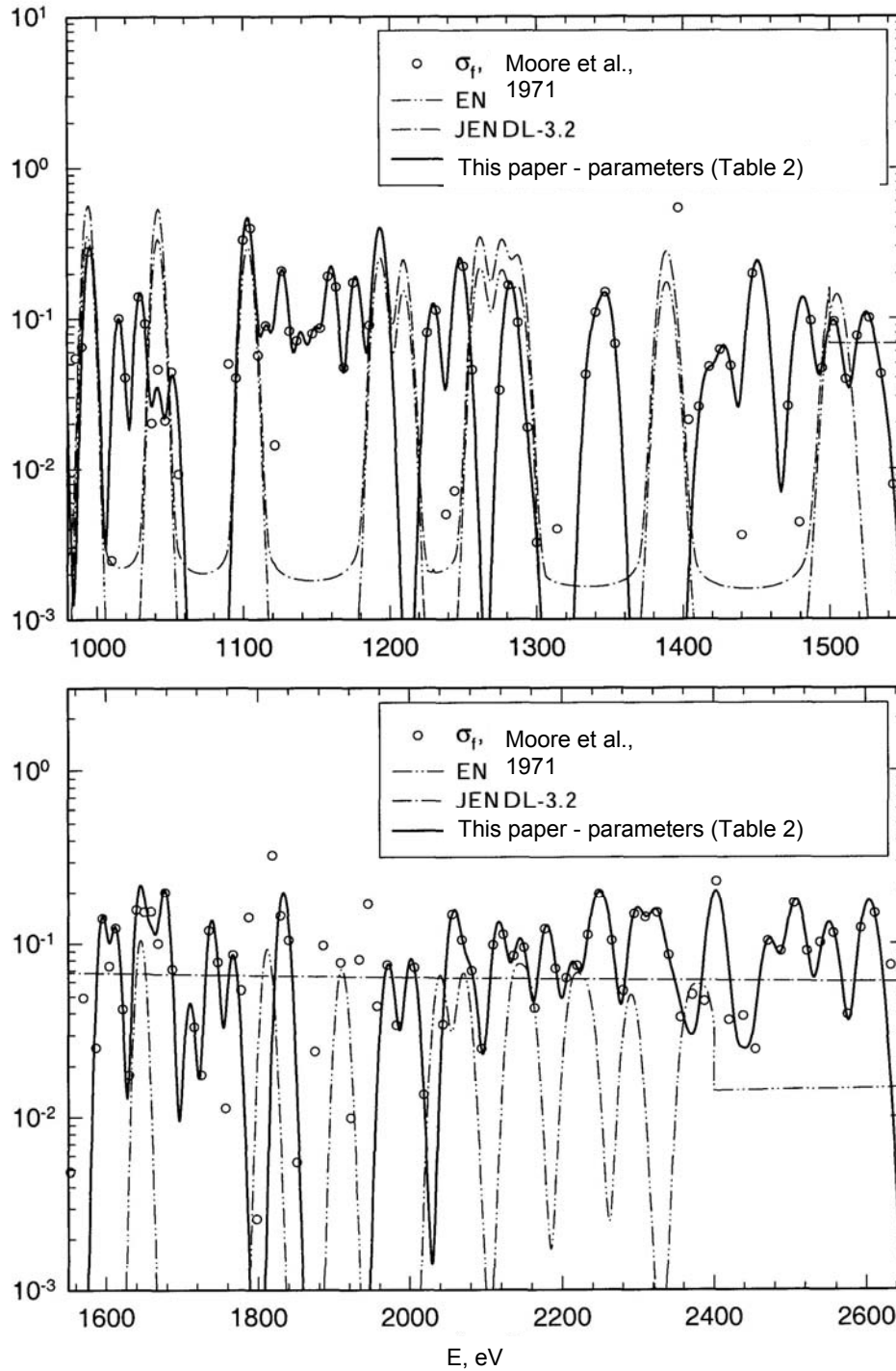
Fig. 5. Comparison of the experimentally measured [2] fission cross-section and the fission cross-sections calculated using the ENDF/B-VI and JENDL-3.3 files and the results of this paper in the 980–2640 eV energy range.

Table 3. Average resonance parameters and thermal cross-sections for ^{248}Cm, calculated using the PSYCHE and INTER programs [11]

	ENDF/B-VI	JENDL-3.3	This paper
$<\Gamma_n^0>$, MeV	6.017	6.365	1.316
$<\Gamma_\gamma>$, MeV	26.16	26.16	20.42
$<\Gamma_f>$, MeV	0.8841	1.3402	1.0135
σ_t , barns	9.064	9.456	14.534
σ_n , barns	6.533	6.514	3.468
σ_γ , barns	2.44	2.57	10.70
σ_f , barns	0.087	0.372	0.365
g_γ	1.00612	1.00572	0.99525
g_f	1.00595	1.00096	0.97260
R ($*10^{-12}$), cm	0.9096	0.910	0.910
$<D>$, eV	52.9723	64.712	13.565
S^0 ($*10^{-4}$)	1.1611	1.0049	0.9751
I_γ , barns	248.340	267.045	279.022[1]
I_f , barns 0. – 20 eV	4.105	0.553	0.922[2] ---------------- 0.961[3]
20 – 2150 eV	4.502	3.236	3.029[2] ---------------- 3.510[3]
0.5–2·10^7 eV	15.419	10.0204	10.183[1] ---------------- 10.703[4]

[1] 0.5 to 2150 eV region – calculation using only the resonance parameters; above 2150 eV – JENDL-3.3 evaluation used

[2] calculation using only the resonance parameters

[3] calculation using the resonance parameters and the smooth background cross-section

[4] 0.5 to 2150 eV region – calculation using the resonance parameters and the smooth background cross-section; above 2150 eV – JENDL-3.3 evaluation used.

Our evaluation of the experimental data [2,3] used in calculation of the parameters, together with the measurements in [2] for ^{245}Cm, which is an admixture in the samples in both experiments, lead us to assume that the aforementioned systematic discrepancy may be due to the fact that the allowance made for this admixture is not absolutely correct. Thus, it follows from [3] that, although the authors made allowance for admixtures in the sample, there is no indication as to how it was done or what data were used. In [2] the authors note that, when measuring the ^{248}Cm fission cross-section, a correction of 1.3% was required for the ^{245}Cm admixture, whereas analysis of the isotopic composition of the sample implied a value of

0.13%. This large increase in the correction could quite easily have resulted in $\sigma_f(E)$ [2] lying systematically lower than the measurements in [3]. Essentially, this "overestimation" of the ^{245}Cm admixture in [2] is, in our view, also the reason why more than 30% of the experimental points have a negative σ_f value, which is considerably more than the usual error for background determination. Since, in absolute terms, the error in the allowance for the admixture in [2] is not large, its influence should be noticeable in the weak resonance region (with relatively small values of $\sigma^0_f(E_r)$) with a sufficiently good energy resolution, and this is what we observe in this case.

Thus, it can be seen in Figs. 1 and 2 that the fairly strong resonances at energies 26.85, 76.1 and 98.85 eV mask this error in the entire 20–100 eV energy range, except for the weak resonance region 30–57 eV. In the 100–550 eV energy range there are also mainly weak resonances such that, if the value of $\sigma^0_f(E_r)$ is averaged over 100 eV ranges, the minimum is in the 100–300 eV region, then there is an increase up to the 600–800 eV region, which is explained by the energy dependence of the discrepancy between the experimental [3] and the calculated fission cross-section values (see Fig. 1), as noted above. The next much weaker minimum is in the 1000–1100 eV region, after which there is an alternation of insignificant rises and falls. It is worth noting, however, that after 700 eV the energy resolution of [2] is such that only strong resonances or clusters, which are represented as a single resonance (the number of missing resonances increases sharply) can be identified, and because of the low resolution of [3] there is a "blurring" of the resonances in a broad energy range, as a result of which the calculation error for the background and the ^{245}Cm admixture becomes insignificant.

The test recalculation that we performed of the correction for the ^{245}Cm admixture for [2] enables agreement between the experimental data in [2 and 3], but this is only our hypothesis. As it is not possible to identify the concrete source (or sources) of the systematic discrepancy between [2 and 3] examined above because of the lack of information about how the measurements were performed, we have compensated for this by means of small additions to the calculated values of the fission cross-section, a so-called "smooth background cross-section", shown in Table 4. This smooth background cross-section is constructed in such a way that the calculated values of the fission cross-sections obtained using our parameters and the experimental conditions of [3] and taking this addition into account were within the error range of the experimental data [3], which can be easily seen in Fig. 1.

Table 4. Smooth background cross-section for the parameters in Table 2

E_i, eV	$\Delta\sigma_f$, barns	E_i, eV	$\Delta\sigma_f$, barns	E_i, eV	$\Delta\sigma_f$, barns
10^{-5}	0.0	65.0	0.0	275.0	0.22
1.250	0.0	92.50	0.0	303.0	0.206
2.960	0.074	111.0	0.384	390.0	0.076
4.0	0.0	125.0	0.48	485.0	0.025
24.0	0.0	178.0	0.33	570.0	0.0
35.0	0.06	210.0	0.34	2150. 0	0.0
55.60	0.06	255.0	0.3		

Table 5. Fission resonance integrals

ΔE, eV	Moore [2]	Maguire [3]	JENDL-3.3	This paper
0.5 – 20	–	0.809[1] ------------- 0.892[2]	0.553	0.922[3] ------------- 0.961[4]
20 – 2150	3.015[1] ------------- 3.296[2]	3.509	3.236	3.029[3] ------------- 3.510[4]

[1]   calculation for all experimental points
[2]   calculation for experimental points without taking account of negative cross-sections
[3]   calculation using only the resonance parameters
[4]   calculation using the resonance parameters and the smooth background cross-section

The considerably larger value of the fission resonance integral in the ENDF/B-VI evaluation compared with JENDL-3.3 and the present paper is due to the fact that the parameters of the first two resonances in the ENDF/B-VI file were not reviewed after the publication of the measurements in [3] (see Fig. 1). However, the discrepancy between the experimental measurements of I_f [9,10] and the JENDL-3.3 value and our study needs to be examined separately. Table 5 gives the calculations of the fission resonance integrals for the experimental measurements [2,3], the JENDL-3.3 file and the present paper. It can be seen from the Table that in the 0.5–20 eV region our parameters accurately reproduce the measurements in [3], unlike the JENDL-3.3 evaluation. In the 20–2150 eV region, the calculation using our parameters is in good agreement with the measurements in [2], which were used to obtain these parameters (in the 20–100 eV region the data in [2,3] are also in good mutual agreement taking into account the energy resolution of the experiments), and the calculation using our parameters with the addition of the smooth background cross-section is in good agreement with the measurement in [3]. Thus, within the 0.5–2150 eV energy region, there is never more than 4.5 b in the total fission resonance integral. Analysis of the ENDF/B-VI and JENDL-3.3 evaluations in the 2150 eV – 20 MeV region shows that they were rather reliably performed, and the magnitudes of I_f are in good mutual agreement (6.8 and 6.2 b, respectively), i.e. the discrepancy with [9,10] is of the order of 2 barns for the entire 0.5 eV–20 MeV region. There are at least three possible reasons for this discrepancy:

- the allowance made for the admixtures in experiments [9,10] is not absolutely correct;

- a similar situation for the experimental data over the high-energy region;

- incorrect data [3] in the region up to 20 eV, which seems unlikely considering the good agreement of the measurements in [2,3] in the 20–100 eV energy range.

Any combination of the above is also possible. The publication of new experimental measurements of the fission cross-section may throw light on the matter.

REFERENCES

1. R.W. Benjamin, C.E. Ahlfeld, J.A. Harvey, N.W. Hill, Nucl. Sci. Eng.. 1974. Vol. 55. p. 440.

2. M.S. Moore, G.A. Keyworth, Phys. Rev. C. 1971. Vol. 3. p. 1656.

3. H.T. Maguire Jr., C.R.S. Stopa, R.C. Block et al., Nucl. Sci. Eng.. 1985. Vol. 89, p. 293.

4. A. Chetham-Strode, R.E. Druschel, J. Halperin, R.J. Silva, P. ORNL-832. 1965. p. 1.

5. R.E. Druschel, R.D. Baybarz, J. Halperin, P. ORNL-4891. 1973. p. 23.

6. T.A. Eastwood, R.P. Schulman, J. Inorg. Nucl. Chem.. 1958. Vol. 6. p. 261.

7. V.D. Gavrilov, V.A. Goncharov, Atomnaya Ehnergiya. 1978. Vol. 44, No. 3, p. 246.

8. G.T. Seaborg, 1955. Private Communication to J.R. Huizenga.

9. R.W. Benjamin, K.W. MacMurdo, J.D. Spencer, Nucl. Sci. Eng.. 1972. Vol. 47. p. 203.

10. K.D. Zhuravlev, N.I. Kroshkin, A.P. Chetverikov, Atomnaya Ehnergiya. 1975. Vol. 39, No. 4. p. 285.

11. C.L. Dunford, ENDF Utility Codes Release 6.9, IAEA-NDS-29. 1993.

MODELLING OF THE TRANSMUTATION OF ATOMIC NUCLEI IN INTENSIVE γ-RAY BEAMS

B.S. Ishkhanov, I.A. Lyutikov, S.I. Pavlov, M.V. Lomonosov Moscow State University, Skobeltsyn Institute of Nuclear Physics, Physics Faculty

MODELLING OF THE TRANSMUTATION OF ATOMIC NUCLEI IN INTENSIVE γ-RAY BEAMS. In this article we consider a mathematical model which describes the intensive bremsstrahlung interaction with atomic nuclei. A program package is proposed to calculate and visualize in automatic mode the formation of transmutation chains for isotopes with 50 < A < 209 within the boundaries of the model. All input parameters may be specified by the user. The code algorithms and user interfaces of the package are described in detail.

INTRODUCTION

To describe the transmutation of atomic nuclei by intensive γ-ray fluxes with energies of 5-30 MeV, a computer program package was created which allows the main physical processes that take place when γ-radiation interacts with atomic nuclei to be modelled.

A feature of this program package is its great dynamic scope and flexibility. This allows the main parameters of the transmutation process that are being modelled to be easily changed: total irradiation time, total observation time, observation interval, γ-ray flux intensity and other essential parameters. In the program's database, information is stored on the decay characteristics of 2500 atomic nuclei, which allows the initial nuclei to be easily varied by setting only the charge Z and mass number A of the isotope to be irradiated.

1.   Description of the Dynamics of the Transmutation of Atomic Nuclei

The basic mechanism of the interaction of photons with atomic nuclei in the 5–30 MeV energy region is excitation and subsequent decay of the giant dipole resonance (GDR) [1, 2].

The model describes the transmutation of atomic nuclei as a result of photonuclear reactions induced by γ-bremsstrahlung beams where the upper limit of the γ-bremsstrahlung spectrum $E_{\gamma m}$ is 30 MeV.

As a result of the irradiation of the initial isotope, a large number of both stable and radioactive isotopes are formed which must be taken into account when examining the transmutation process. Characteristic radioactive decays for the region of atomic nuclei being studied (50 < A < 210) are β⁻-, β⁺- and α-decays.

The evolution over time of the quantity of each element in the transmutation chain $N_{(A,Z)}(t)$ is determined by its accumulation and decay processes. Reduction in the content of the isotope (A, Z) occurs as a result of the *(γ, n), (γ, 2n)* and *(γ, p)* reactions and in α- and β-decay

processes. Accumulation of (A, Z) nuclei occurs as a result of photonuclear reactions on neighbouring isotopes, and α- and β-decays of neighbouring isotopes, as a result of which the isotope in question (A, Z) may be formed (see Fig. 1).
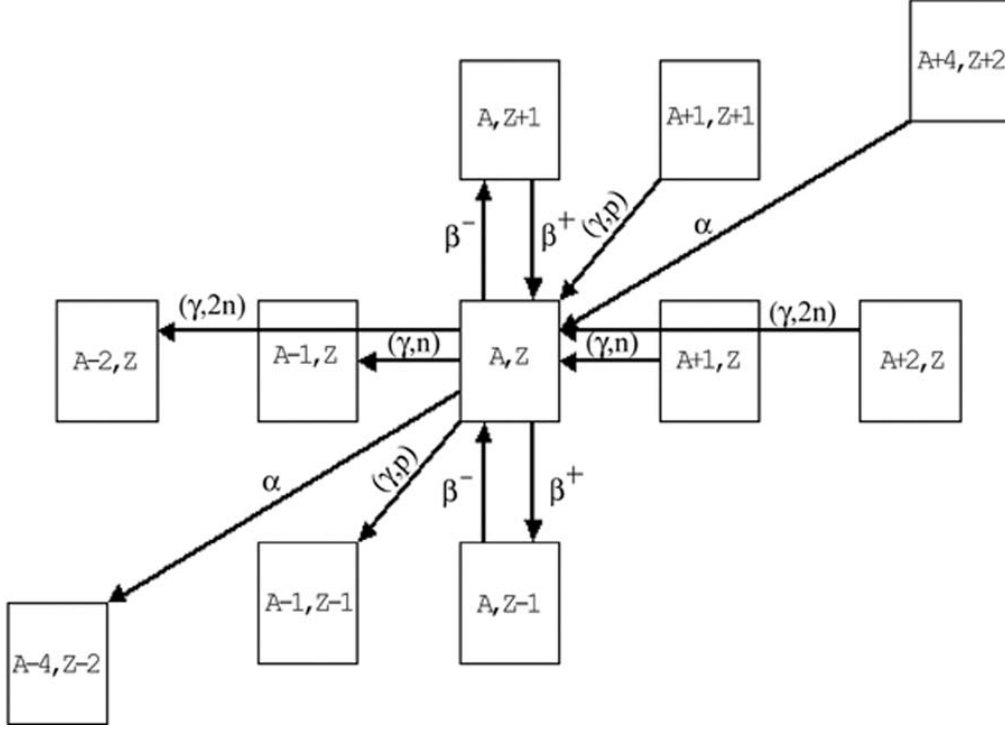
Fig. 1. Diagram of the formation of transmutation chain elements

The evolution over time of the quantity of an isotope $N_{(A,Z)}(t)$ is described using the following equation:

$$\frac{dN_{(A,Z)}(t)}{dt} = -\left[\lambda_{(A,Z)}^{\beta^-} + \lambda_{(A,Z)}^{\beta^+} + \lambda_{(A,Z)}^{\alpha} + Y_{(A,Z)}^{(\gamma,n)} + Y_{(A,Z)}^{(\gamma,2n)} + Y_{(A,Z)}^{(\gamma,p)} \right] N_{(A,Z)}(t) +$$

$$\left\{ \lambda_{(A,Z-1)}^{\beta^-} N_{(A,Z-1)}(t) + \lambda_{(A,Z+1)}^{\beta^+} N_{(A,Z+1)}(t) + \lambda_{(A+4,Z+2)}^{\alpha} N_{(A+4,Z+2)}(t) \right\} + \qquad (1)$$

$$\left\{ + Y_{(A+1,Z)}^{(\gamma,n)} N_{(A+1,Z)}(t) + Y_{(A+2,Z)}^{(\gamma,2n)} N_{(A+2,Z)}(t) + Y_{(A+1,Z+1)}^{(\gamma,p)} N_{(A+1,Z+1)}(t) \right\}$$

The activity of an isotope $A_{(A,Z)}(t)$ at the point in time t is determined using the following equation:

$$A_{(A,Z)}(t) = \left[\lambda_{(A,Z)}^{\beta^-} + \lambda_{(A,Z)}^{\beta^+} + \lambda_{(A,Z)}^{\alpha} \right] N_{(A,Z)}(t) \qquad (2)$$

The terms in square brackets in differential equation (1) describe the destruction of the isotope in the photonuclear reactions *(γ, n)*, *(γ, 2n)* and *(γ, p)* and in α- and β-decay processes. The terms in braces describe the formation of the isotope in *(γ, n)*, *(γ, 2n)* and *(γ, p)* reactions from neighbouring isotopes and in α- and β-decay processes.

Equations (1) and (2) contain the following parameters:

$\lambda^i_{(A,Z)}$ — decay constant of the isotope (A, Z) for the channel i, where i stands for α-, β⁻- and β⁺- decays;

$Y^j_{(A,Z)}(E_{\gamma m})$ — yield of a photonuclear reaction on the isotope (A,Z) determined using the following equation:

$$Y^j_{(AZ)}(E_{\gamma m}) = \Phi(photons \cdot s^{-1}) \int_{E_{min}}^{E_{\gamma m}} W(E,E_{\gamma m})\sigma^j_{(A,Z)}(E)dE, \qquad (3)$$

where j corresponds to the channels of the *(γ, n), (γ ,2n)* and *(γ, p)* reactions on the isotope (A, Z);

Φ (photons · s⁻¹) is the flux density of the photons irradiating the target mode of the isotope being studied;

$\sigma^j_{(A,Z)}(E)$ is the partial cross-section of the photonuclear reaction j.

Integration in equation (3) is performed in the nucleus excitation energy region from $E_{min} = 5$ MeV, which corresponds to the minimum photonuclear reaction threshold values, to the upper boundary of the γ-bremsstrahlung spectrum $E_{\gamma m}$, which was set at 30 MeV.

2.   Gamma Bremsstrahlung Spectrum

Modelling of the bremsstrahlung from targets of finite thickness was performed using the GEANT program package [3].

In all calculations of transmutation chains, the γ-bremsstrahlung spectrum formed by irradiation of a tungsten target was used. The target thickness was set at 0.4 cm, which corresponds to the effective length of the path of the electrons in tungsten.

Figure 2 shows an example of a bremsstrahlung spectrum of γ-rays formed by the interaction of electrons with an energy of E_e=30 MeV with a tungsten target.
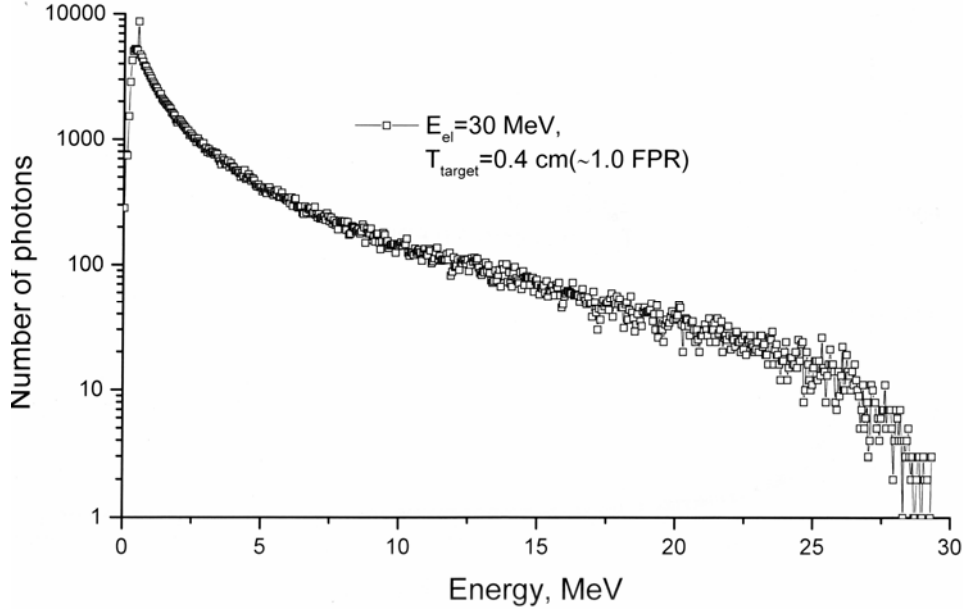
Fig. 2. Example of a bremsstrahlung spectrum calculated using GEANT

3.   Description of Photonuclear Reaction Cross-sections

To describe the evolution over time of nuclei in transmutation chains, data on the cross-sections of photonuclear reactions and on the β⁻-, β⁺- and α-decay of the product nuclei are needed. At present, detailed information is available on the rate of β⁻-, β⁺- and α-decay. However, data on the cross-sections of photonuclear reactions are only available for nuclei located along the stability line. Data have been obtained on photoneutron reactions for isotopes in the mass number region $A < 210$, while data on the photoproton channel are generally limited to nuclei with $A < 60$.

The shape of the cross-section in the GDR region of medium and heavy nuclei is adequately approximated by a Lorentzian (Fig. 3)

$$\sigma(E) = \frac{\sigma_m}{1 + \frac{(E^2 - E^{m2})^2}{E^2 \Gamma^2}},\tag{5}$$

where E is the photon energy, E^m is the position of the centre of mass of the giant dipole resonance, Γ is the width of the giant dipole resonance and σ_m is the cross-section value at the photoabsorption maximum.

To approximate the energy dependence of the photoabsorption cross-section, the following information on the GDR parameters is required:

1.   the position of the GDR maximum — E^m;

2.   the cross-section value at the photoabsorption maximum — σ_m;

3.   the width of the GDR — Γ.

26
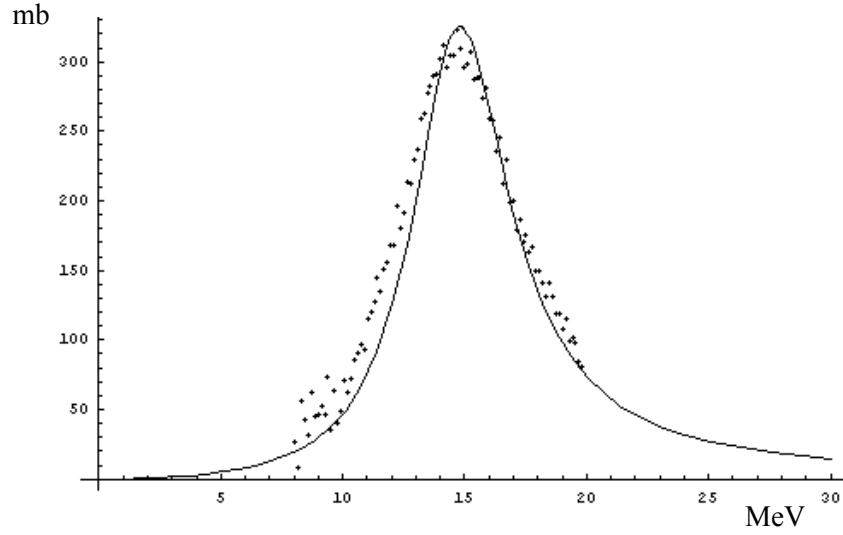
Fig. 3. Shape of the GDR and its approximation using formula (5) for the ^{150}Sm isotope

Figure 4 shows the experimentally measured dependence of the centre of mass E^m of the GDR on the mass number A and the results of two different approximations of the position of the centre of mass of the GDR ((6a), (6b)).

$$E^m = 78A^{-\frac{1}{3}} (MeV); \tag{6a}$$

$$E^m = 31.2A^{-\frac{1}{3}} + 20.6A^{-\frac{1}{6}} (MeV). \tag{6b}$$
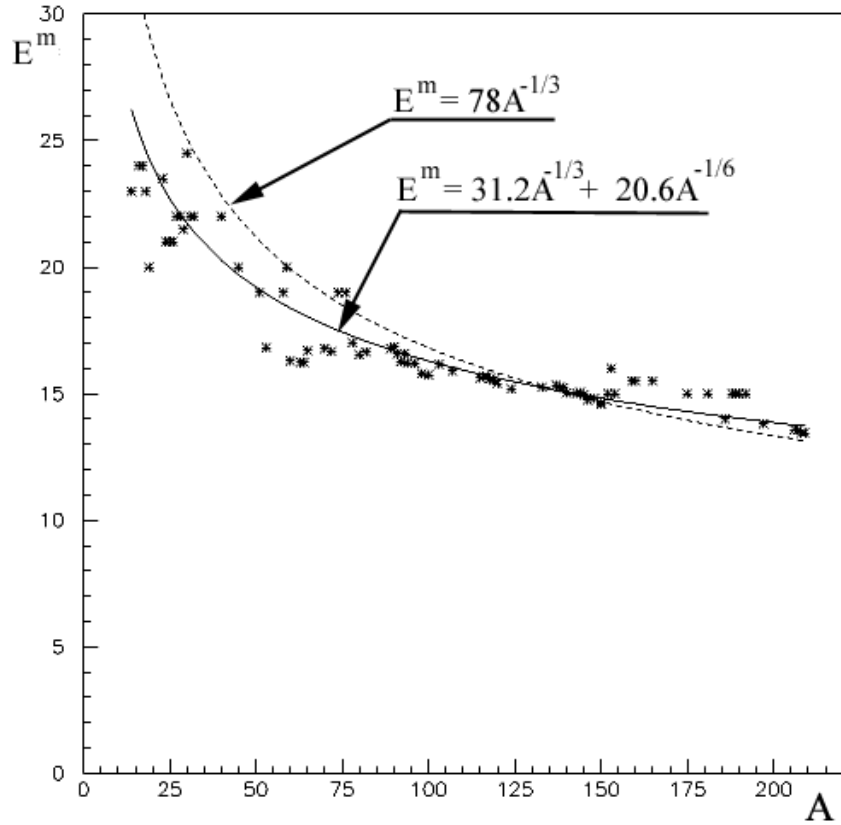
Fig. 4. Experimental values for the centre of mass of the GDR E^m and results of approximations using equations (6a) and (6b)

It is clear from Fig. 4 that, for medium and heavy nuclei (A>60), the differences between the two approximation curves are small and both describe adequately the experimental data according to the position of the centre of mass of the GDR.

The total integrated cross-section for photon interaction with atomic nuclei in the GDR region $\sigma_{int}(\gamma, tot)$ is determined as the sum of the cross-sections of the following main reaction channels:

$$\sigma_{int}(\gamma, \ tot) = \sigma_{int}(\gamma, \ n) + \sigma_{int}(\gamma, \ 2n) + \sigma_{int}(\gamma, \ p) + \sigma_{int}(\gamma, \ 3n) + \sigma_{int}(\gamma, \ np).$$

Figure 5 shows the total cross-section $\sigma_{int}(\gamma, tot)$ and reaction cross-sections $\sigma_{int}(\gamma, n)$, $\sigma_{int}(\gamma, 2n)$ and $\sigma_{int}(\gamma, 3n)$ relative to the mass number A. The dotted line shows the approximation of the total absorption cross-section using the dipole sum rule:

$$\sigma_{int}(\gamma, \ tot) = 60 \ \frac{NZ}{A}(MeV \times mb) \tag{7}$$

The continuous lines show the linear approximation of the integrated reaction cross-sections $\sigma_{int}(\gamma, n)$ and $\sigma_{int}(\gamma, 2n)$ relative to the mass number A. It should be noted that the spread of experimentally measured integrated cross-section values is not only due to measurement error but also to the different cross-section integration limits in the different references.

28
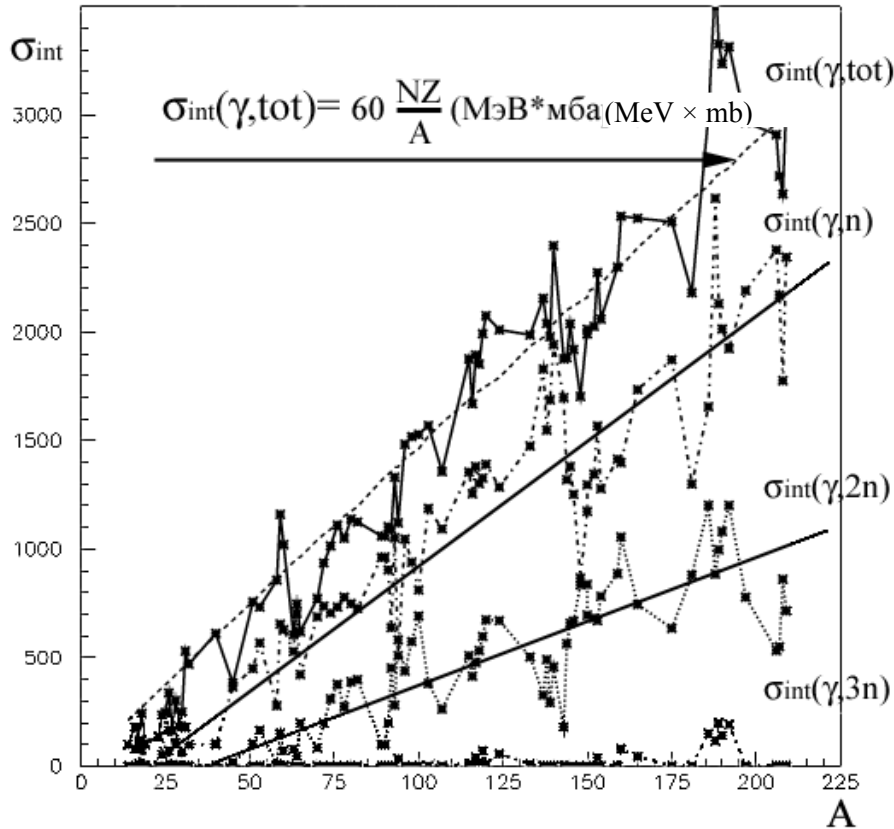
Fig. 5. Dependence of the integrated photonuclear reaction cross-sections on the mass number A. The total cross-section $\sigma_{int}(\gamma, tot)$ is shown and the reaction cross-sections $\sigma_{int}(\gamma, n)$, $\sigma_{int}(\gamma, 2n)$ and $\sigma_{int}(\gamma, 3n)$. The dotted lines show the approximation of the total absorption cross-section using the dipole sum rule; the continuous lines show the linear approximation for the integrated cross-sections $\sigma_{int}(\gamma, n)$ and $\sigma_{int}(\gamma, 2n)$

Research into the influence of various factors on the measurement and subsequent reconstruction of photonuclear reaction cross-sections has shown that the main factors are as follows:

1. Method of obtaining the cross-sections — use of a photon or quasi-monochromatic photon bremsstrahlung spectrum [4];

2. Dependence of the efficiency of the recording instrument on the energy of the particles being recorded;

3. Accuracy of measurement of the upper boundary of the bremsstrahlung spectrum;

4. Energy resolution of the quasimonochromatic photon spectrum and influence of the low-energy base.

As a result, the difference between the actual accuracy and the one given in the publications can be up to 10–20%, which constitutes the systematic error of the experiment.

When developing the program, the following parameters for describing the cross-sections of γ-ray interaction with atomic nuclei were selected to perform calculations:

1. The total integrated photoabsorption cross-section was determined using equation (7).

2. The cross-section value at the photoabsorption maximum σ_m is described using the equation:

$$\sigma_m = \frac{1}{\displaystyle\int_{E_{\min}}^{E_{\gamma m}} \frac{1}{1 + \dfrac{(E^2 - E^{m^2})^2}{E^2 \Gamma^2}}} \times \varsigma; \quad \frac{N Z}{A}. \tag{8}$$

3. The dependence of the total absorption cross-section on the energy E in the GDR region was described using equation (5):

$$\sigma(E) = \frac{\sigma_m}{1 + \dfrac{(E^2 - E^{m^2})^2}{E^2 \Gamma^2}}, \tag{9}$$

where E is the photon energy, E^m is the position of the centre of mass of the GDR, Γ is the width of the GDR and σ_m is the cross-section value at the photoabsorption maximum. The energy dependence of the cross-section is the same for all types of photonuclear reaction taken into account in the model;

4. The position of the centre of mass of the GDR E^m was described using equation (6b);

5. The width of the GDR was set as $\Gamma \sim 5$ MeV and varied within the limits ± 1 MeV;

6. In line with the experimental data on photonuclear reaction cross-sections in the A ~ 70-210 mass number region, for all isotopes formed the following relative cross-section values were selected for the different reaction channels irrespective of A and Z:

   – (γ, n) reaction channel: ~70% of the total absorption cross-section;
   – (γ, 2n) reaction channel: ~25% of the total absorption cross-section;
   – (γ, p) reaction channel: ~5% of the total absorption cross-section;

7. The more complex GDR decay channels were not taken into account.

The cross-sections and yields of the relevant photonuclear reactions were calculated using the method described.

Figure 6 compares the γ-ray absorption cross-sections calculated by us and those measured experimentally in the GDR energy region for various isotopes of lead ($^{206,\ 207,\ 208}$Pb), bismuth (^{209}Bi), tungsten ($^{182,\ 184,\ 186}$W,) and yttrium (^{89}Y). It is clear from Fig. 6 that the energy dependence of the experimentally measured cross-sections are adequately described using the models proposed by us even for deformed nuclei ($^{182,\ 184,\ 186}$W). The aim of the model described above was not to provide a detailed description of the shape of the absorption cross-section but a maximal approximation of the shape of the cross-section by one Lorentzian, in order to obtain the yields of the relevant reactions with a sufficient degree of accuracy.

The fourth column of Table 1 gives the differences between the yields of the photoabsorption reaction calculated using experimental data Y_{exp} and the yields calculated in the proposed model Y_{mod} for a bremsstrahlung spectrum with an upper energy boundary of 30 MeV. The fifth and six columns of the table give the integration boundaries for each isotope.
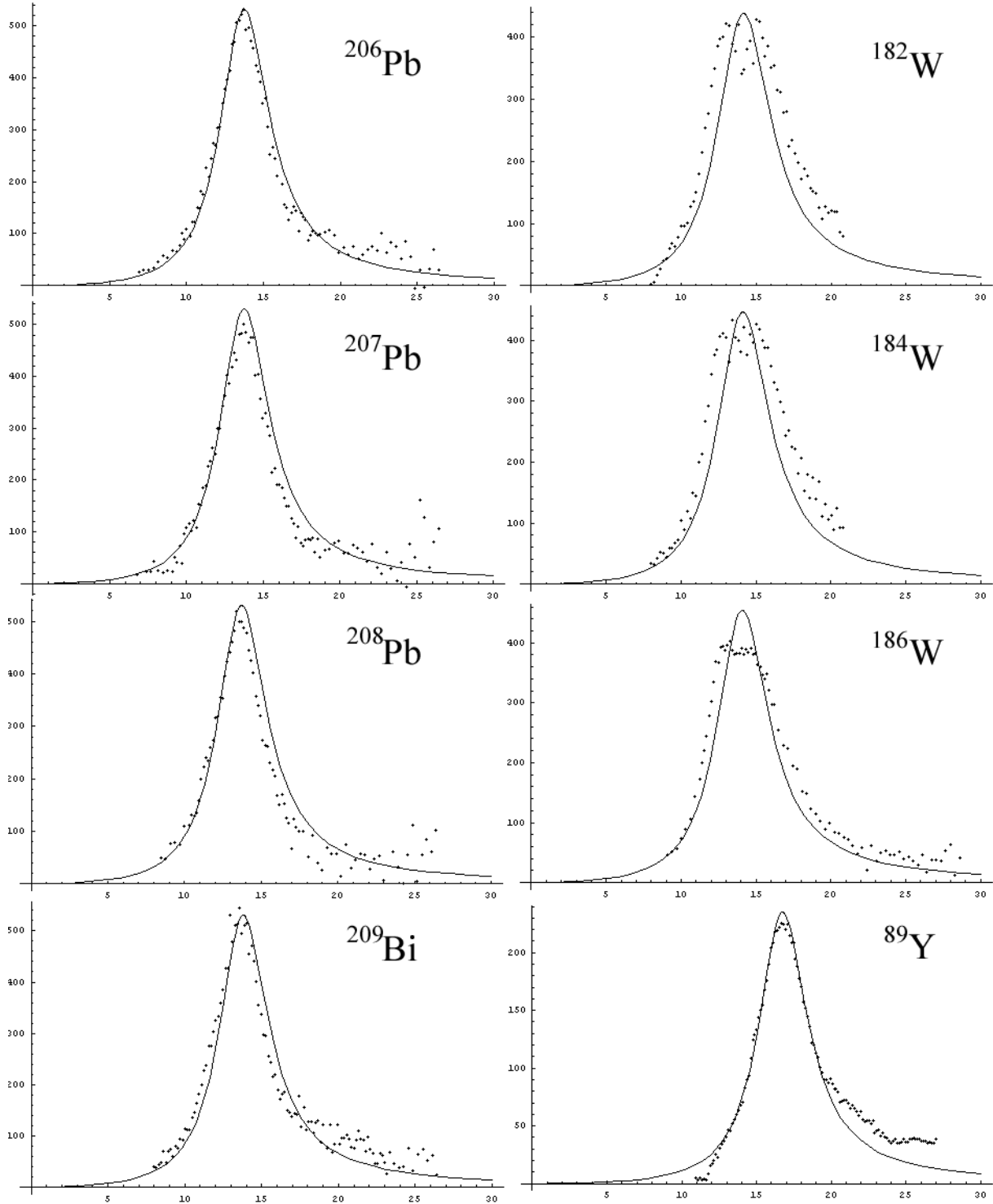
Fig. 6. Photoabsorption cross-section plotted using experimental data (dots) and calculated using the proposed method (continuous lines). Cross-sections measured in mb, energy in MeV.

The maximum difference for all photonuclear reaction yields given in Table 1 is ~19%. Similar assessments of yield calculation accuracy were performed for other nuclei for which data on the reaction cross-sections were available. They characterize the accuracy of the method used by us.

Table 1. Comparison of photoabsorption reaction yields calculated using experimental data Y_{exp} with yields calculated in the model in question Y_{mod} for a bremsstrahlung spectrum with an upper energy boundary of 30 MeV

Z	Element	A	$\dfrac{\lvert Y_{\text{мод}} - Y_{\text{эксп}} \rvert}{Y_{\text{эксп}}} \times 100\%$	E_{min}, MeV	E_{max}, MeV
82	Pb	206	1.66	6.929	26.441
82	Pb	207	8.88	6.775	26.441
82	Pb	208	6.98	8.478	26.441
83	Bi	209	3.12	8.013	26.441
74	W	182	17.5	8.02	20.82
74	W	184	19.3	8.02	20.82
74	W	186	10.5	9.097	26.608
39	Y	89	0.163	10.948	27.02

4.   Software

To study the transmutation of atomic nuclei by intensive γ-ray fluxes, a program package was used which allows a transmutation chain to be constructed and calculated in automatic mode using given starting parameters. The programs included in this package can be divided provisionally into two modules — a calculation module and a visualization module. At high γ-ray flux intensities and extensive irradiation times, a large number of isotopes are formed in the transmutation chain (up to several hundred), which greatly increases the calculation time (up to 24 hours). This was the reason why the program package was divided into two modules.

Calculation module. An important part of this module is the electronic databases containing information on decay constants and photonuclear reaction yields for nuclei formed as a result of the transmutation of the initial isotope. The database was created using an electronic version of the decay constants nuclear database of the Centre for Photonuclear Experiments Data [5]. To create a database containing information on photonuclear reaction yields, a set of utilities was developed which, based on data on the bremsstrahlung spectrum calculated using the GEANT program, and using a phenomenological model for describing photonuclear reaction cross-sections, allows photonuclear reaction yield values for the whole range of nuclei covered by the phenomenological model to be calculated and entered in the database. The transmutation chains are constructed, and calculations of the evolution over time of the content and activity of the elements in the transmutation chain for the initial nuclei are performed by numerically solving equations (1) and (2), taking into account the various physical restrictions imposed by the scope of the model and using the information contained

in the databases. To control construction of the transmutation chain, the parameter $L(t)$ — leakage — was introduced, which may be determined using the following equation:

$$L(t) = \left(1 - \frac{\sum N_{(A,Z)}(t)}{N_0}\right) \cdot 100\%, \tag{10}$$

where N_0 is the original number of nuclei and $N_{(A,Z)}(t)$ is the number of nuclei of (A, Z) in the chain at the point in time t. $L(t)$ is the relative number of nuclei that have passed beyond the boundaries of the construction of the chain in the transmutation process at a given point in time.

Interface description. The calculation program window is shown in Fig. 7. The program window displays the following entry and command parameters:

- Start A — the mass number A of the initial isotope;

- Start Z — the charge Z of the initial isotope;

- N — original number of nuclei of the initial isotope (A, Z);

- eps — maximum leakage $L(t)$ for this calculation, measured in relative units;

- Phi — bremsstrahlung photon flux density (photons $\cdot$ s^{-1});

- Channel panel — inclusion/exclusion of the relevant reaction channels for this calculation;

- $(\gamma, n),(\gamma, 2n)$ and (γ, p) slide bars — to change the ratios of the photonuclear reaction channels for each specific calculation;

- SetStop — to switch on/off calculation optimization mode;

- Accuracy for each nucleus — selected when calculating reactions with a low-intensity gamma-ray flux;

- K — coefficient for converting the base time units for use in DeltaTime. The original base unit is the second. A coefficient of 3600 makes the base unit an hour;

- DeltaTime — determines the time interval after which information obtained from the calculation of the evolution of the transmutation chain is recorded into the output text files;

- AllTime — determines the total calculation time, including irradiation time and observation time after irradiation;

- EndRadiat — determines the time when irradiation ends in DeltaTime units;

- InitCount — used to ensure that the actual calculation of the chain begins only after the number of nuclei in the chaint is greater than or equal to the InitCount (used to optimize program operation for large flux densities or a long irradiation time).

    The program outputs the following results in the form of text data files:

33

- numbers of the nuclei in the transmutation chain, their mass numbers *A* and charges *Z*;

- numerical data on the quantity of all nuclei in the transmutation chain at a given time interval;

- numerical data on the activity of different isotopes, and the total activity of all isotopes in the transmutation chain at a given time interval;

- numerical data on the evolution of the mass number and charge distribution densities of *Ap* and *Zp*.

The text files produced can be converted into MS Excel tables to perform a statistical analysis and plot graphs. Moreover, by assembling these text files in a different way, independent databases can be created.
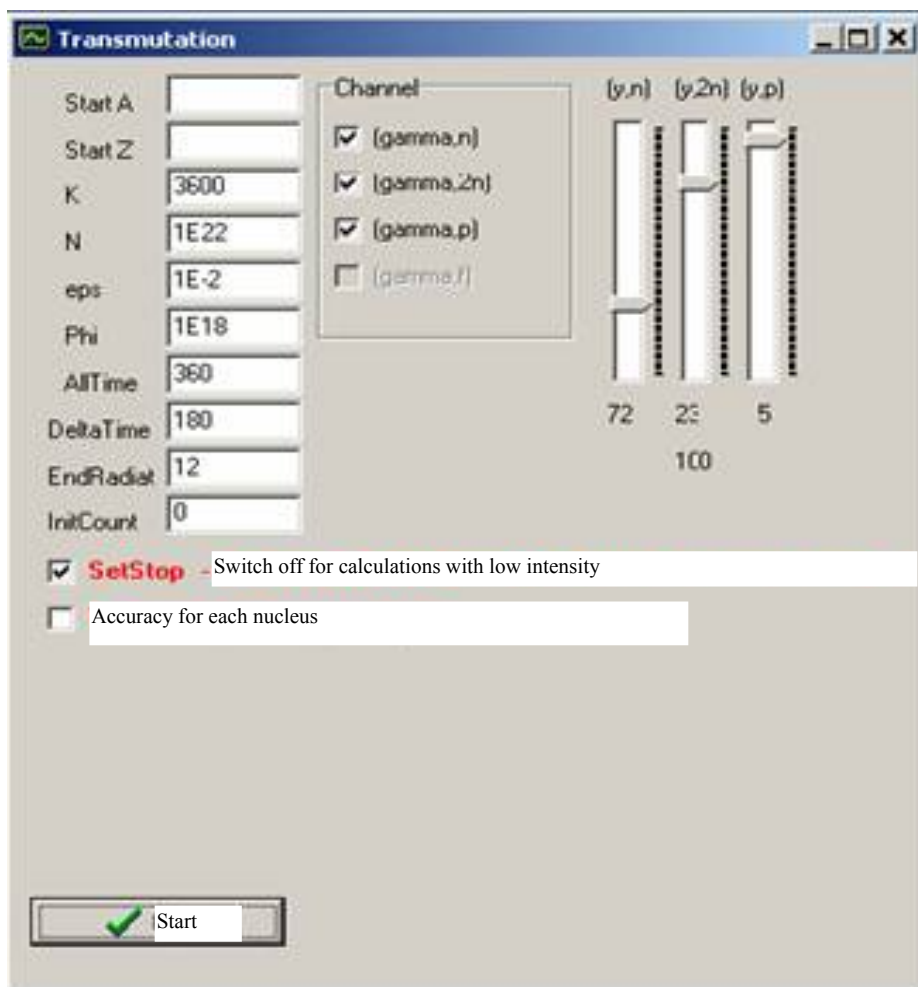
Fig. 7. Calculation program window.

Visualization module. This program module can be used to observe the dynamic process of transmutation chain formation. The database containing the information on the isotopes formed in the transmutation process and their quantity-time dependence is created using the data files from the calculation module.

Interface description. Figure 8 shows the program window. The program comprises a demonstration area and a control panel. The control panel contains the following items:

- Four drop-down boxes:

  - Element — box with a drop-down list of the chemical elements in the program database with the charge *Z* indicated in brackets;

  - Mass number, A — box with a drop-down list of the mass numbers in the program database corresponding to the selected element;

  - Gamma ray flux, Φ — box with a drop-down list of the γ-ray flux intensity values in the program database corresponding to the selected element and mass number;

  - Irradiation time — box with a drop-down list of the irradiation times in the program database corresponding to the selected element, mass number and γ-ray flux intensity;
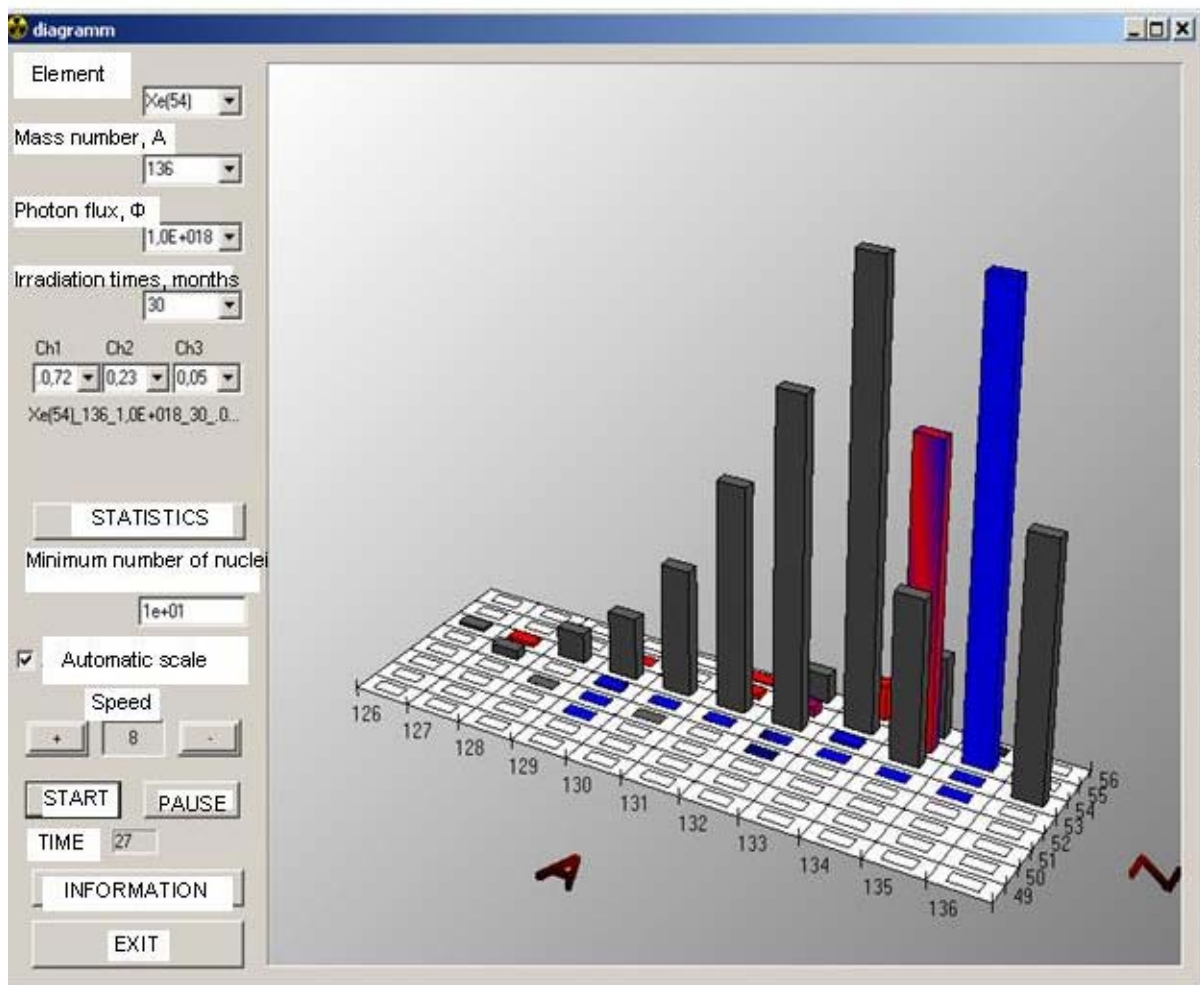
Fig. 8. Visualization module window

- "n; 2, n; n, p" — three drop-down boxes in which the user selects the available ratios between the photonuclear reaction channels;

- STATISTICS — pressing this button opens a text file containing information on all isotopes in the transmutation chain and their quantities at the end of irradiation and the end of observation;

35

- Minimum number of nuclei — in this box, a number corresponding to the minimum number of isotopes represented in the diagram is entered;

- Automatic scale — ticking this box automatically selects the scale of the axis corresponding to the number of isotopes. If it is not ticked, the change in the height of the columns corresponds to the real changes in the number of isotopes;

- +/– — speeds up/slows down the modelling process;

- START — initiates the modelling process;

- PAUSE — pressing this button stops the modelling process; pressing it again resumes the modelling process;

- TIME — time elapsed since the start of the irradiation process in the units selected in the irradiation time dialog box;

- INFORMATION — output of reference and theoretical material;

- EXIT — exits the program.

The dynamic image is constructed in the demonstration window of the program which is a three-dimensional (*A, Z,* number) graphical space. *A* is the mass number of the isotope. *Z* is the charge of the isotope. The number of nuclei of the given isotope is determined by the height of the columns. The columns are in three colours: black, red and blue. The columns corresponding to stable isotopes are coloured black, β^+-radioactive isotopes are red and β^--radioactive isotopes are blue. Those with two types of activity have blue/red gradient colouring. The image construction area can be rotated by pressing and holding down the left mouse button. The size of the program window is changed using the mouse.

CONCLUSION

The program package created allows transmutation chains of isotopes with $50 < A < 209$ to be automatically constructed and calculated using set parameters. The possibility is offered of using different shapes and upper boundaries of the γ-ray spectra for the calculations. The calculation module program outputs the following data as text files:

- number of a nucleus in chain, its mass number and charge;

- quantity/time data on nuclei in the transmutation chain;

- data on the time dependence of the total activity of the isotopes, and different isotopes in the transmutation chain;

- data on the transmutation trajectory.

The files obtained can be used for direct analysis of transmutation chains, to convert them into any graphics packages and to plot dependence graphs, and to create a database containing information on the formation of transmutation chains of different isotopes for various practical applications. One such application is the database created on the transmutation of stable isotopes with $50 < A < 209$. The results of calculations for 220 stable isotopes have been entered in the database. The modelling was carried out for the following conditions: photon flux — 10^{18} photons/s; irradiation time of isotopes being studied — 30 months; total

observation time, including radiation time — 90 months. The ratios of the photoabsorption reaction channels were selected as follows: (γ, n) — 72%, (γ, 2n) — 23%, (γ, p) — 5%. This database is used by the visualization module program, allowing the formation of the transmutation chain and the change in the number of nuclei of each isotope in the chain to be followed dynamically.

REFERENCES

1. Ishkhanov, B.S., Kapitonov, I.M., Neudachin, V.G., et al., Configurational splitting of the giant dipole resonance in atomic nuclei, Uspekhi Fizicheskikh Nauk, 1990, vol. 160, pp. 67–99 [in Russian].

2. Ishkhanov, B.S., Kapitonov, I.M., Ehramzhyan, R.A., Study of the giant dipole resonance in (γ, xγ´) experiments, Fizika Ehlementarnykh Chastits i Atomnogo Yadra, 1992, vol. 23, pp. 1770–1826 [in Russian].

3. Burn, R., Bruyant, F., Maire, M., et al., GEANT 3.21 (User's Guide), CERN, Geneva, Switzerland, 1987.

4. Varlamov, V.V., Ishkhanov, B.S., The giant dipole resonance in various types of photonuclear experiment: divergences, causes, means of elimination, consequences, Fizika Ehlementarnykh Chastits i Atomnogo Yadra, 2004, vol. 35(4), pp. 858–894.

5. Centre for Photonuclear Experiments Data, Skobeltsyn Institute of Nuclear Physics, Moscow State University, *http://depni.npi.msu.ru/cdfe/*